Composite Structures 187 (2018) 566–578

Contents lists available at ScienceDirect

Composite Structures

journal homepage: www.elsevier.com/locate/compstruct

Explicit tangent stiffness matrix for the geometrically nonlinear analysis of laminated composite frame structures

Ardalan R. Sofi[a], Peter L. Bishay[a,*], Satya N. Atluri[b]

[a] California State University, Northridge, CA, USA
[b] Texas Tech University, Lubbock, TX, USA

ARTICLE INFO

Keywords:
Large deformation
Updated Lagrangian
Finite elements
Composite beams

ABSTRACT

In this paper, based on Von Kármán's nonlinear theory and the classical lamination theory, a closed form expression is derived for the tangent stiffness matrix of a laminated composite beam element undergoing large deformation and rotation under mechanical and hygrothermal loads. Stretching, bending and torsion have been considered. A co-rotational element reference frame is used as the Updated Lagrangian (UL) formulation. The model has been verified in different problems by comparison with the results of Nastran and ANSYS composite laminate tools, and the difference in the resulting large deformations is less than 5%. The major advantage of the proposed approach is that the composite structure is modeled using 1D beam elements rather than 2D shell or 3D solid elements as in the case of Nastran and ANSYS where laminates are defined over surfaces or 3D solids. The availability of an explicit expression for the tangent stiffness matrix makes the proposed model highly efficient specially when dealing with large composite space frame structures. The saving in computational time could reach 93% compared to regular FE software packages. The developed model is very useful for modeling and designing flexible composites used in new applications such as morphing aerospace structures and flexible robots.

1. Introduction

With the appearance of new technologies and inventions in the fields of automotive design, aerospace structures, smart structures, and robotics, the design and manufacturing of laminated composite materials have seen a lot of development. Beside the well-known applications of fiber-reinforced laminated composite materials because of their various advantages, such as high specific stiffness and strength, high corrosion resistance, good thermal insulation, fatigue resistance and damping properties, new applications of composite materials emerged that necessitate the development of new effective and efficient tools and approaches in design and simulation. For example, a lot of smart material elements, such as shape memory alloy (SMA) wires or ribbons and piezoelectric patches or fibers, are embedded in polymer composite laminates to form smart composite structures with multi-functions such as sensing, actuating and load bearing [1–3]. Another example is the design of morphing aerospace structures, such as morphing wings with flexible seamless control surfaces or flexible winglets [4]. The design of such structures is challenging because of the need to have flexible, yet strong, wing skins that can morph to different shapes and still be able to stand aerodynamic loads. Composite actuators combining shape memory wires, glass fibers in a soft matrix that could morph into complex shapes utilizing coupling effects for in-plane, out-of-plane, and twisting deformations have been proposed [5–7] and applied to interesting applications such as turtle-like swimming robot [8] and morphing car spoiler [9]. Another example is robotic arms and manipulators made of flexible laminated composite end-effectors [10,11]. Flexible composites are manufactured as reinforcing fibers in flexible matrix. Such flexible composites undergo large deformations, hence for modeling these structures, geometric nonlinearity should be considered. In addition, composite beams and plates with high slenderness ratios, normally undergo large displacements and rotations even without reaching large strains and/or overcoming the material's elastic limit [12]. Hence, it is critical to develop computational tools to efficiently and accurately predict the deformation of such composite structures subjected to any mechanical or hygrothermal loads. This will also be very useful in the design process where large number of iterations are to be done sweeping the parameters in the design space to achieve the desired goals.

Introducing geometric nonlinearity to structures is an option in almost all available commercial finite element software nowadays, such as ANSYS, ABAQUS, and MSC Nastran. Defining a composite layup

* Corresponding author.
E-mail address: peter.bishay@csun.edu (P.L. Bishay).

https://doi.org/10.1016/j.compstruct.2017.11.006
Received 17 August 2017; Received in revised form 21 September 2017; Accepted 6 November 2017
Available online 12 November 2017

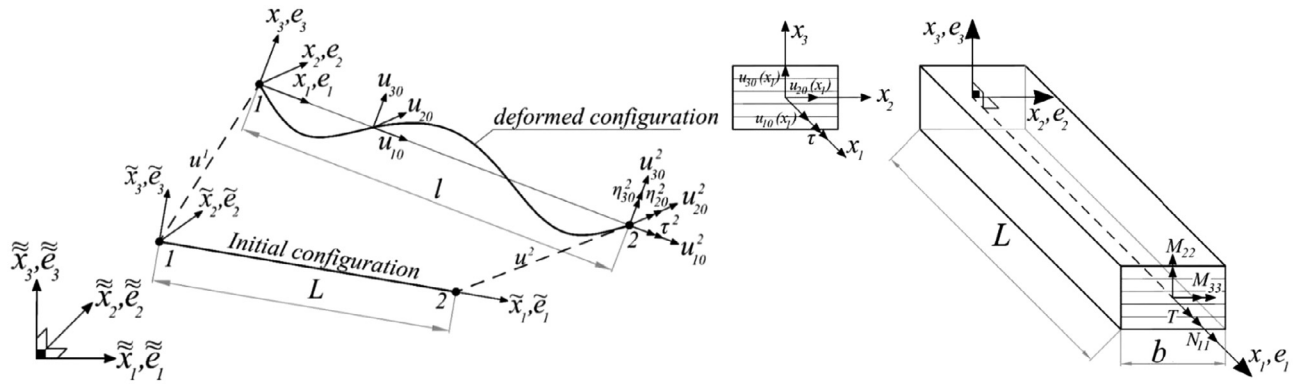

Fig. 1. (left) Kinematic diagram of the laminated composite 3D beam element, (right) Laminated composite beam subjected to torsion, bending moments and axial force.

given the material properties of all plies, their fiber orientations and thicknesses can also be done in all the aforementioned software in addition to SOLIDWORKS Simulation, Autodesk Simulation Mechanical, and Nastran-in-CAD tool integrated in any CAD software such as SOLIDWORKS or Autodesk Inventor. Composite laminates are defined in these software on a surface or 3D solid to be meshed using 2D plate or shell elements or 3D solid elements, respectively. Composite laminates cannot be defined on lines to model beams or 3D frames. Hence, the computational cost of performing geometrically nonlinear static or dynamic analyses on large composite structures, such as trusses, frames or idealized structures, becomes very high. The development of a 3D frame element for the geometric nonlinear analysis of laminated composite beams will then be very effective and efficient due to the expected simplicity and low computational costs.

Several three-dimensional frame finite element formulations for the geometric nonlinear analysis of thin-walled laminated composite beams have been developed during the last two decades. Bhaskar and Librescu [13,14] developed nonlinear theory of thin-walled composite beams with closed and open sections taking into account the transverse shear deformation effect while the warping torsion component was neglected. Omidvar and Ghorbanpoor [15] and Cardoso et al. [16] proposed a three-dimensional nonlinear finite element models for thin-walled open-section composite beams with symmetric stacking sequence, including the warping effect, and based on the Updated Lagrangian (UL) formulation. Based on Von Kármán strain tensor, Vo and Lee [17,18] developed three-dimensional thin-walled laminated beam elements with open sections, and investigated the effects of fiber orientation, geometric nonlinearity, and shear deformation on the axial–flexural–torsional response. Mororó et al. [12] developed three-dimensional thin-walled laminated beam elements with closed sections using Total Lagrangian (TL) formulation allowing large displacements and moderate rotations, but without the effects of warping and transverse shear. Saravia [18] developed consistent large deformation-small strain formulation for thin-walled composite beams (TWCB) calling it a "geometrically exact TWCB formulation" suitable for modeling high aspect ratio composite beams that undergo large rigid body motions, such as wind turbine wings, satellite arms and automotive body stiffeners. Turkalj [20] presented a beam formulation for large displacement analysis of composite frames considering the flexibility of the connections.

Atluri and his co-workers extensively studied large rotations in beams, plates and shells, and attendant variational principles (see [21–24]). Explicit derivations of the tangent stiffness matrix of 3D frames including elasto-plasticity were derived [25–27] without employing either numerical or symbolic integrations. Based on a Von Kármán type nonlinear theory in rotated reference frames, Cai et al. [28] developed a simple geometrically nonlinear large-rotation beam element with arbitrary cross-section using a co-rotational reference frame for each finitely rotated beam element as the UL reference frame for the respective element, and accounting for stretching, bending and torsion. An explicit expression of a symmetric tangent stiffness matrix of the beam element in the co-rotational frame was derived and validated in multiple numerical examples of space frames undergoing large deformations.

Even in the simplest formulation of the aforementioned works that presented geometrically nonlinear composite beams [12–20], an explicit expression for the tangent stiffness matrix could not be reached. Hence in this work, a finite element formulation of laminated composite beams undergoing large deformation and rotation, in response to mechanical or hygrothermal loads, is developed based on Von Kármán nonlinear theory and the classical lamination theory. Stretching, bending, and torsion has been accounted for, and a closed form expression of the element tangent stiffness matrix has been derived, utilizing the element's co-rotational reference frame as the UL formulation. The model has been verified in different problems by comparison with Nastran and ANSYS results. In all problems, the difference in the resulting deformations is less than 5%. The relative simplicity of the derived explicit tangent stiffness matrix is one of the major advantages of the proposed approach, which makes large deformation analyses of laminated composite beams highly efficient specially when dealing with large composite space frame structures.

2. Transformation between the global and the deformation-dependent co-rotational local frames of reference

Consider a beam element made up of fiber-reinforced composite laminate in the initial configuration and then deforms to the deformed configuration when loads are applied on it, as shown in Fig. 1 (left). The global coordinate system is denoted $\widetilde{x}_1$–$\widetilde{x}_2$–$\widetilde{x}_3$, with $\widetilde{e}_1$–$\widetilde{e}_2$–$\widetilde{e}_3$ as the unit vectors in the directions of the three global axes. $\widetilde{x}_1$–$\widetilde{x}_2$–$\widetilde{x}_3$ and x_1–x_2–x_3 are the coordinate syst of the initial and deformed configurations respectively, with corresponding unit vectors $\widetilde{e}_1$–$\widetilde{e}_2$–$\widetilde{e}_3$ and e_1–e_2–e_3, respectively as shown in Fig. 1 (left).

The unit vectors of the initial configuration are defined as follows: $\widetilde{e}_1$ is simply defined using the nodal coordinates of the element's two end nodes,

$$\widetilde{e}_1 = (\Delta\widetilde{x}_1\widetilde{e}_1 + \Delta\widetilde{x}_2\widetilde{e}_2 + \Delta\widetilde{x}_3\widetilde{e}_3)/L, \tag{1}$$

where $\Delta\widetilde{x}_1 = \widetilde{x}_1^{(2)} - \widetilde{x}_1^{(1)}$; $\Delta\widetilde{x}_2 = \widetilde{x}_2^{(2)} - \widetilde{x}_2^{(1)}$; $\Delta\widetilde{x}_3 = \widetilde{x}_3^{(2)} - \widetilde{x}_3^{(1)}$; $L = \sqrt{(\Delta\widetilde{x}_1)^2 + (\Delta\widetilde{x}_2)^2 + (\Delta\widetilde{x}_3)^2}$, and the superscript (j) in $\widetilde{x}_i^{(j)}$ indicates the node number.

$\widetilde{e}_2$ is perpendicular to $\widetilde{e}_3$ and $\widetilde{e}_1$, while $\widetilde{e}_3$ is perpendicular to $\widetilde{e}_1$ and $\widetilde{e}_2$:

$$\widetilde{e}_2 = (\widetilde{e}_3 \times \widetilde{e}_1)/|\widetilde{e}_3 \times \widetilde{e}_1| = (-\Delta\widetilde{x}_2\widetilde{e}_1 + \Delta\widetilde{x}_1\widetilde{e}_2)/Z; \quad \widetilde{e}_3 = \widetilde{e}_1 \times \widetilde{e}_2, \tag{2}$$

where $Z = \sqrt{(\Delta\widetilde{x}_1)^2 + (\Delta\widetilde{x}_2)^2}$.

Therefore, the relation between $\widetilde{e}_1,\widetilde{e}_2,\widetilde{e}_3$ and $\widetilde{\widetilde{e}}_1,\widetilde{\widetilde{e}}_2,\widetilde{\widetilde{e}}_3$ could be written in matrix form as:

$$\begin{Bmatrix}\widetilde{e}_1\\ \widetilde{e}_2\\ \widetilde{e}_3\end{Bmatrix} = \frac{1}{ZL}\begin{bmatrix} Z\Delta\widetilde{x}_1 & Z\Delta\widetilde{x}_2 & Z\Delta\widetilde{x}_3\\ -L\Delta\widetilde{x}_2 & L\Delta\widetilde{x}_1 & 0\\ -\Delta\widetilde{x}_1\Delta\widetilde{x}_3 & -\Delta\widetilde{x}_2\Delta\widetilde{x}_3 & Z^2\end{bmatrix}\begin{Bmatrix}\widetilde{\widetilde{e}}_1\\ \widetilde{\widetilde{e}}_2\\ \widetilde{\widetilde{e}}_3\end{Bmatrix} \tag{3}$$

The unit vectors in the directions of the deformed configuration coordinates are defined as follows: e_1 depends on the nodal coordinates of the deformed beam element,

$$e_1 = (\Delta x_1\widetilde{\widetilde{e}}_1 + \Delta x_2\widetilde{\widetilde{e}}_2 + \Delta x_3\widetilde{\widetilde{e}}_3)/l, \tag{4}$$

where $\Delta x_1 = x_1^{(2)} - x_1^{(1)}$; $\Delta x_2 = x_2^{(2)} - x_2^{(1)}$; $\Delta x_3 = x_3^{(2)} - x_3^{(1)}$; $l = \sqrt{(\Delta x_1)^2 + (\Delta x_2)^2 + (\Delta x_3)^2}$. e_2 is perpendicular to $\widetilde{e}_3$ and e_1, while e_3 is perpendicular to e_1 and e_2:

$$e_2 = (\widetilde{e}_3 \times e_1)/|\widetilde{e}_3 \times e_1|; \quad e_3 = e_1 \times e_2. \tag{5}$$

Now, e_1 and $\widetilde{e}_3$ can be written as:

$$e_1 = a_1\widetilde{\widetilde{e}}_1 + a_2\widetilde{\widetilde{e}}_2 + a_3\widetilde{\widetilde{e}}_3; \quad \widetilde{e}_3 = c_1\widetilde{\widetilde{e}}_1 + c_2\widetilde{\widetilde{e}}_2 + c_3\widetilde{\widetilde{e}}_3, \tag{6}$$

where $a_1 = \frac{\Delta x_1}{l}$; $a_2 = \frac{\Delta x_2}{l}$; $a_3 = \frac{\Delta x_3}{l}$, and $c_1 = \frac{-\Delta\widetilde{x}_1\Delta\widetilde{x}_3}{ZL}$; $c_2 = \frac{-\Delta\widetilde{x}_2\Delta\widetilde{x}_3}{ZL}$; $c_3 = \frac{Z}{L}$.

Using Eq. (5), e_2 could be expressed as:

$$\begin{aligned} e_2 &= [(c_2a_3 - c_3a_2)\widetilde{\widetilde{e}}_1 + (c_3a_1 - c_1a_3)\widetilde{\widetilde{e}}_2 + (c_1a_2 - c_2a_1)\widetilde{\widetilde{e}}_3]/l^*\\ &= b_1\widetilde{\widetilde{e}}_1 + b_2\widetilde{\widetilde{e}}_2 + b_3\widetilde{\widetilde{e}}_3, \end{aligned} \tag{7}$$

where $l^* = \sqrt{(c_2a_3 - c_3a_2)^2 + (c_3a_1 - c_1a_3)^2 + (c_1a_2 - c_2a_1)^2}$ and $b_1 = \frac{c_2a_3 - c_3a_2}{l^*}$; $b_2 = \frac{c_3a_1 - c_1a_3}{l^*}$; $b_3 = \frac{c_1a_2 - c_2a_1}{l^*}$.

Finally e_3 takes the form:

$$e_3 = (a_2b_3 - a_3b_2)\widetilde{\widetilde{e}}_1 + (a_3b_1 - a_1b_3)\widetilde{\widetilde{e}}_2 + (a_1b_2 - a_2b_1)\widetilde{\widetilde{e}}_3 \tag{8}$$

Therefore, the relationship between e_1,e_2,e_3 and $\widetilde{\widetilde{e}}_1,\widetilde{\widetilde{e}}_2,\widetilde{\widetilde{e}}_3$ is written in matrix form as

$$\begin{Bmatrix}e_1\\ e_2\\ e_3\end{Bmatrix} = \boldsymbol{\lambda}_0\begin{Bmatrix}\widetilde{\widetilde{e}}_1\\ \widetilde{\widetilde{e}}_2\\ \widetilde{\widetilde{e}}_3\end{Bmatrix}; \quad \text{where } \boldsymbol{\lambda}_0 = \begin{bmatrix} a_1 & a_2 & a_3\\ b_1 & b_2 & b_3\\ (a_2b_3 - a_3b_2) & (a_3b_1 - a_1b_3) & (a_1b_2 - a_2b_1)\end{bmatrix}. \tag{9}$$

$\boldsymbol{\lambda}_0$ is the transformation matrix between e_1,e_2,e_3 and $\widetilde{\widetilde{e}}_1,\widetilde{\widetilde{e}}_2,\widetilde{\widetilde{e}}_3$.

3. Von Kármán nonlinear theory for a beam with large deformation

As shown in Fig. 1 (right), the laminated composite beam is subjected to torsion T about x_1 direction, and bending moments M_{22} and M_{33} about x_3 and x_2 directions, respectively. The cross-sectional area is assumed to be constant throughout the deformation of the composite beam. The displacements of the beam's centerline are denoted $u_{10}(x_1)$, $u_{20}(x_1)$, $u_{30}(x_1)$. The bending deformations resulting from M_{33} and M_{22} are $x_3(\partial u_{30}/\partial x_1)$ and $x_2(\partial u_{20}/\partial x_1)$ respectively. The total torsion of the beam about x_1 due to the torque T is denoted $\tau(x_1)$.

With the above definitions and Fig. 1 (right), it is possible to write three equations for the total displacements of the composite beam in x_1, x_2 and x_3 directions:

$$\begin{aligned} u_1 &= u_{10}(x_1) - x_2\frac{\partial u_{20}}{\partial x_1} - x_3\frac{\partial u_{30}}{\partial x_1}; \quad u_2 = u_{20}(x_1) - x_3\tau(x_1); \quad u_3\\ &= u_{30}(x_1) + x_2\tau(x_1). \end{aligned} \tag{10}$$

3.1. Strain-displacement relations

Green-Lagrange strain-displacement relations describing the large deformations of the thin composite beam based on Von Kármán's nonlinear theory take the following forms: Axial strain in the x_1 direction:

$$\begin{aligned} \varepsilon_{11} &= \frac{\partial u_1}{\partial x_1} + \frac{1}{2}\left[\left(\frac{\partial u_1}{\partial x_1}\right)^2 + \left(\frac{\partial u_2}{\partial x_1}\right)^2 + \left(\frac{\partial u_3}{\partial x_1}\right)^2\right] = \frac{\partial u_{10}}{\partial x_1} - x_2\frac{\partial^2 u_{20}}{\partial x_1^2} - x_3\frac{\partial^2 u_{30}}{\partial x_1^2}\\ &\quad + \frac{1}{2}\left[\left(\frac{\partial u_{10}}{\partial x_1} - x_2\frac{\partial^2 u_{20}}{\partial x_1^2} - x_3\frac{\partial^2 u_{30}}{\partial x_1^2}\right)^2 + \left(\frac{\partial u_{20}}{\partial x_1}\right)^2 + \left(\frac{\partial u_{30}}{\partial x_1}\right)^2\right]\\ &= u_{10,1} + x_2[X_{22} + (u_{10,1})X_{22}] + x_3[X_{33} + (u_{10,1})X_{33}] + \frac{1}{2}x_2^2(X_{22}^2)\\ &\quad + \frac{1}{2}x_3^2(X_{33}^2) + \frac{1}{2}x_2x_3X_{22}X_{33} + \frac{1}{2}[(u_{10,1})^2 + (u_{20,1})^2 + (u_{30,1})^2], \end{aligned} \tag{11}$$

where the notations $u_{i0,j} = \frac{\partial u_{i0}}{\partial x_j}$ and $X_{ii} = -u_{i0,11} = -\frac{\partial^2 u_{i0}}{\partial x_1^2}$ are used. The terms that contain $(u_{10,1})^2$, $(u_{10,1})X_{22}$, $(u_{10,1})X_{33}$, X_{22}^2, X_{33}^2 and $X_{22}X_{33}$ are assumed to be very small compared to X_{22}, X_{33} and $u_{10,1}$. Therefore, these terms are neglected in the further development of the strain-displacement relations. ε_{11} is then expressed as,

$$\varepsilon_{11} = \varepsilon_{11}^0 + x_2X_{22} + x_3X_{33}, \tag{12}$$

where

$$\varepsilon_{11}^0 = u_{10,1} + \frac{1}{2}[(u_{20,1})^2 + (u_{30,1})^2] = \varepsilon_{11}^{0L} + \varepsilon_{11}^{0N} \tag{13}$$

Similarly, the other normal and shear strain components are expressed as:

$$\begin{aligned} \varepsilon_{22} &= \frac{\partial u_2}{\partial x_2} + \frac{1}{2}\left[\left(\frac{\partial u_1}{\partial x_2}\right)^2 + \left(\frac{\partial u_2}{\partial x_2}\right)^2 + \left(\frac{\partial u_3}{\partial x_2}\right)^2\right]\\ &= 0 + \frac{1}{2}\left[\left(-\frac{\partial u_{20}}{\partial x_1}\right)^2 + 0 + \tau^2\right] = \frac{1}{2}[(u_{20,1})^2 + \tau^2], \end{aligned} \tag{14}$$

$$\begin{aligned} \varepsilon_{33} &= \frac{\partial u_3}{\partial x_3} + \frac{1}{2}\left[\left(\frac{\partial u_1}{\partial x_3}\right)^2 + \left(\frac{\partial u_2}{\partial x_3}\right)^2 + \left(\frac{\partial u_3}{\partial x_3}\right)^2\right]\\ &= 0 + \frac{1}{2}\left[\left(-\frac{\partial u_{30}}{\partial x_1}\right)^2 + 0 + \tau^2\right] = \frac{1}{2}[(u_{30,1})^2 + \tau^2], \end{aligned} \tag{15}$$

$$\varepsilon_{23} = \frac{1}{2}\left(\frac{\partial u_2}{\partial x_3} + \frac{\partial u_3}{\partial x_2}\right) = \frac{1}{2}(-\tau + \tau) = 0, \tag{16}$$

$$\varepsilon_{31} = \frac{1}{2}\left(\frac{\partial u_1}{\partial x_3} + \frac{\partial u_3}{\partial x_1}\right) = \frac{1}{2}\left(-\frac{\partial u_{30}}{\partial x_1} + \frac{\partial u_{30}}{\partial x_1} + \frac{\partial \tau}{\partial x_1}x_2\right) = \frac{1}{2}(\eta x_2) \tag{17}$$

$$\varepsilon_{12} = \frac{1}{2}\left(\frac{\partial u_1}{\partial x_2} + \frac{\partial u_2}{\partial x_1}\right) = \frac{1}{2}\left(-\frac{\partial u_{20}}{\partial x_1} + \frac{\partial u_{20}}{\partial x_1} - \frac{\partial \tau}{\partial x_1}x_3\right) = \frac{1}{2}(-\eta x_3) \tag{18}$$

where $\eta = \frac{\partial \tau}{\partial x_1}$. The strain tensor written in matrix form can now be written as linear and nonlinear components:

$$\boldsymbol{\varepsilon} = \boldsymbol{\varepsilon}^L + \boldsymbol{\varepsilon}^N, \tag{19}$$

$$\begin{aligned} \boldsymbol{\varepsilon}^L &= \begin{Bmatrix}\varepsilon_{11}^L\\ \varepsilon_{22}^L\\ \varepsilon_{33}^L\\ \gamma_{23}^L\\ \gamma_{31}^L\\ \gamma_{12}^L\end{Bmatrix} = \begin{bmatrix}u_{10,1}\\ 0\\ 0\\ 0\\ 0\\ 0\end{bmatrix} + x_2\begin{bmatrix}X_{22}\\ 0\\ 0\\ 0\\ \eta\\ 0\end{bmatrix} + x_3\begin{bmatrix}X_{33}\\ 0\\ 0\\ 0\\ 0\\ -\eta\end{bmatrix}, \quad \boldsymbol{\varepsilon}^N = \begin{Bmatrix}\varepsilon_{11}^N\\ \varepsilon_{22}^N\\ \varepsilon_{33}^N\\ \gamma_{23}^N\\ \gamma_{31}^N\\ \gamma_{12}^N\end{Bmatrix}\\ &= \frac{1}{2}\begin{bmatrix}(u_{20,1})^2 + (u_{30,1})^2\\ (u_{20,1})^2 + \tau^2\\ (u_{30,1})^2 + \tau^2\\ 0\\ 0\\ 0\end{bmatrix} \end{aligned} \tag{20}$$

where $\gamma_{ij} = 2\varepsilon_{ij}$ $(i \neq j)$ are the engineering shear strains. As shown in Eq. (20), ε_{22} and ε_{33} do not have any linear terms and their nonlinear terms

are relatively small. Therefore, these normal strains that are perpendicular to the beam's longitudinal direction could be neglected, and the linear and nonlinear strains can be reduced to:

$$\boldsymbol{\varepsilon}^L = \begin{bmatrix} \varepsilon_{11}^L \\ \gamma_{31}^L \\ \gamma_{12}^L \end{bmatrix} = \begin{bmatrix} u_{10,1} \\ 0 \\ 0 \end{bmatrix} + x_2 \begin{bmatrix} \mathrm{X}_{22} \\ \eta \\ 0 \end{bmatrix} + x_3 \begin{bmatrix} \mathrm{X}_{33} \\ 0 \\ -\eta \end{bmatrix}, \quad \boldsymbol{\varepsilon}^N = \begin{bmatrix} \varepsilon_{11}^N \\ \gamma_{31}^N \\ \gamma_{12}^N \end{bmatrix} = \frac{1}{2} \begin{bmatrix} (u_{20,1})^2 + (u_{30,1})^2 \\ 0 \\ 0 \end{bmatrix} \tag{21}$$

3.2. Stress-strain relations

Considering each composite lamina to have linear elastic material behavior, the additional second Piola-Kirchhoff stress tensor written in matrix form could be written as [29]:

$$\boldsymbol{\sigma}^1 = \overline{\mathbf{Q}}\boldsymbol{\varepsilon}, \tag{22}$$

where $\boldsymbol{\sigma}^1 = [\sigma_{11}^1 \ \sigma_{22}^1 \ \sigma_{33}^1 \ \sigma_{23}^1 \ \sigma_{31}^1 \ \sigma_{12}^1]^T$, $\boldsymbol{\varepsilon} = [\varepsilon_{11} \ \varepsilon_{22} \ \varepsilon_{33} \ \gamma_{23} \ \gamma_{31} \ \gamma_{12}]^T$ and

$$\overline{\mathbf{Q}} = \overline{\boldsymbol{\Psi}}^{-1} = (\mathbf{T}^T\boldsymbol{\Psi}\mathbf{T})^{-1} = \mathbf{T}^{-1}\boldsymbol{\Psi}^{-1}\mathbf{T}^{-T}, \tag{23}$$

$$\boldsymbol{\Psi} = \begin{bmatrix} \frac{1}{E_{x'}} & \frac{-\nu_{x'y'}}{E_{x'}} & \frac{-\nu_{x'z'}}{E_{x'}} & 0 & 0 & 0 \\ \frac{-\nu_{y'x'}}{E_{y'}} & \frac{1}{E_{y'}} & \frac{-\nu_{y'z'}}{E_{y'}} & 0 & 0 & 0 \\ \frac{-\nu_{z'x'}}{E_{z'}} & \frac{-\nu_{z'y'}}{E_{z'}} & \frac{1}{E_{z'}} & 0 & 0 & 0 \\ 0 & 0 & 0 & \frac{1}{G_{y'z'}} & 0 & 0 \\ 0 & 0 & 0 & 0 & \frac{1}{G_{z'x'}} & 0 \\ 0 & 0 & 0 & 0 & 0 & \frac{1}{G_{x'y'}} \end{bmatrix}; \quad \mathbf{T} = \begin{bmatrix} c^2 & s^2 & 0 & 0 & 0 & \sin 2\theta \\ s^2 & c^2 & 0 & 0 & 0 & -\sin 2\theta \\ 0 & 0 & 1 & 0 & 0 & 0 \\ 0 & 0 & 0 & c & -s & 0 \\ 0 & 0 & 0 & s & c & 0 \\ -sc & sc & 0 & 0 & 0 & c^2-s^2 \end{bmatrix}$$

$E_{x'}, E_{y'}, E_{z'}$ are the three Young's moduli, $\nu_{x'y'}, \nu_{y'z'}, \nu_{z'x'}$ are the three Poisson's ratios, and $G_{x'y'}, G_{y'z'}, G_{z'x'}$ are the three shear moduli in the local axes of the orthotropic lamina shown in Fig. 2 (right). $c = \cos\theta$ and $s = \sin\theta$.

As was mentioned earlier, ε_{22}, ε_{33} and γ_{23} strains are neglected, hence we do not consider the associated stresses. The stress-strain relations in a single lamina can then be written as

$$\begin{Bmatrix} \sigma_{11}^1 \\ \sigma_{31}^1 \\ \sigma_{12}^1 \end{Bmatrix} = \begin{Bmatrix} \sigma_{11}^{1L} \\ \sigma_{31}^{1L} \\ \sigma_{12}^{1L} \end{Bmatrix} + \begin{Bmatrix} \sigma_{11}^{1N} \\ \sigma_{31}^{1N} \\ \sigma_{12}^{1N} \end{Bmatrix} = \begin{bmatrix} \overline{Q}_{11} & \overline{Q}_{15} & \overline{Q}_{16} \\ \overline{Q}_{51} & \overline{Q}_{55} & \overline{Q}_{56} \\ \overline{Q}_{61} & \overline{Q}_{56} & \overline{Q}_{66} \end{bmatrix} \left(\begin{Bmatrix} \varepsilon_{11}^L \\ \gamma_{31}^L \\ \gamma_{12}^L \end{Bmatrix} + \begin{Bmatrix} \varepsilon_{11}^N \\ \gamma_{31}^N \\ \gamma_{12}^N \end{Bmatrix} \right) \tag{24}$$

Fig. 2 (left) shows the cross section of the composite beam made up of n laminae, where each lamina could be made of different material and have different fiber orientation angle θ_k. The total thickness of the laminate is $h = \sum_{i=1}^{n} t_i$ and the location of the top and bottom surfaces of ply k are expressed as:

$$h_{k-1} = -\frac{h}{2} + \sum_{i=1}^{i=k-1} t_i \quad \text{(top)}; \quad h_k = -\frac{h}{2} + \sum_{i=1}^{i=k} t_i \quad \text{(bottom)} \tag{25}$$

where $k = 2,3,\ldots,n-2,n-1$.

The nodal axial force in the beam's longitudinal direction (x_1-direction) could be expressed as

$$N_{11} = N_{11}^L + N_{11}^N = \int_A (\sigma_{11}^{1L} + \sigma_{11}^{1N}) dA \tag{26}$$

Using Eqs. (24) and (21), we can write the linear component of N_{11} as

$$\begin{aligned} N_{11}^L = \int_A \sigma_{11}^{1L} dA = \int_A \Big[& \overline{Q}_{11}u_{10,1} + x_2\overline{Q}_{11}\mathrm{X}_{22} + x_2\overline{Q}_{15}\eta + x_3\overline{Q}_{11}\mathrm{X}_{33} \\ & - x_3\overline{Q}_{16}\eta \Big] dx_2 dx_3 \simeq \sum_{k=1}^{n} \Big[bu_{10,1} \int_{h_{k-1}}^{h_k} \overline{Q}_{11} dx_3 + b\mathrm{X}_{33} \int_{h_{k-1}}^{h_k} \overline{Q}_{11} x_3 dx_3 \\ & - b\eta \int_{h_{k-1}}^{h_k} \overline{Q}_{16} x_3 dx_3 \Big] \simeq bu_{10,1} \sum_{k=1}^{n} \overline{Q}_{11} \Big(h_k - h_{k-1} \Big) \\ & + \frac{b}{2}\mathrm{X}_{33} \sum_{k=1}^{n} \overline{Q}_{11} \Big(h_k^2 - h_{k-1}^2 \Big) - \frac{b}{2}\eta \sum_{k=1}^{n} \overline{Q}_{16} \Big(h_k^2 - h_{k-1}^2 \Big). \end{aligned} \tag{27}$$

where the term $\int_A (\overline{Q}_{11}\mathrm{X}_{22} + \overline{Q}_{15}\eta) x_2 dx_2 dx_3$ vanishes because the integration in x_2 direction is always from $-b/2$ to $b/2$. Similarly, the nonlinear component of N_{11} becomes

$$\begin{aligned} N_{11}^N = \int_A \sigma_{11}^{1N} dA &= \int_A \frac{1}{2}\overline{Q}_{11}((u_{20,1})^2 + (u_{30,1})^2) dx_2 dx_3 \\ &\simeq \sum_{k=1}^{n} \frac{b}{2}((u_{20,1})^2 + (u_{30,1})^2) \int_{h_{k-1}}^{h_k} \overline{Q}_{11} dx_3 \\ &\simeq \frac{b}{2}((u_{20,1})^2 + (u_{30,1})^2) \sum_{k=1}^{n} \overline{Q}_{11}(h_k - h_{k-1}). \end{aligned} \tag{28}$$

The axial force, N_{11} can then be written as:

$$N_{11} = N_{11}^L + N_{11}^N \simeq b\hat{A}\varepsilon_0^{11} + b\hat{C}\mathrm{X}_{33} - b\hat{D}\eta, \tag{29}$$

where

$$\hat{A} = \sum_{k=1}^{n} \overline{Q}_{11}(h_k - h_{k-1}); \quad \hat{C} = \frac{1}{2}\sum_{k=1}^{n} \overline{Q}_{11}(h_k^2 - h_{k-1}^2); \quad \hat{D} = \frac{1}{2}\sum_{k=1}^{n} \overline{Q}_{16}(h_k^2 - h_{k-1}^2), \tag{30}$$

The nodal bending moments about x_2 and x_3 (M_{33} and M_{22}), and the nodal torque about x_1 (T) can be developed similarly to get:

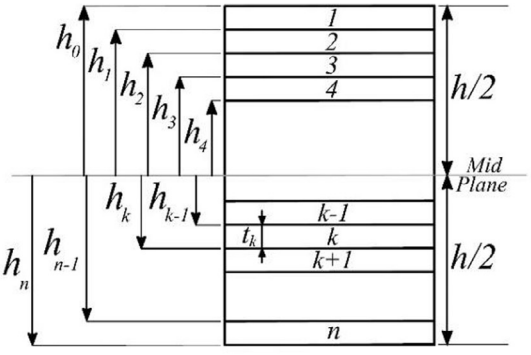

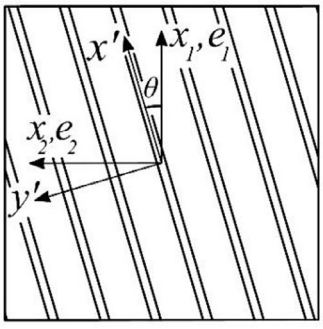

Fig. 2. Schematic of the laminated fiber-reinforced composite beam cross section (left), and fiber orientation in a single lamina (right).

$$M_{33} = M_{33}^L + M_{33}^N = \int_A \left(\sigma_{11}^{1L} + \sigma_{11}^{1N}\right) x_3 dA \simeq b\hat{C}\varepsilon_0^{11} + b\hat{F}\mathrm{X}_{33} - b\hat{G}\eta, \tag{31}$$

$$M_{22} = M_{22}^L + M_{22}^N = \int_A \left(\sigma_{11}^{1L} + \sigma_{11}^{1N}\right) x_2 dA = \frac{b^3}{12}\hat{A}\mathrm{X}_{22} + \frac{b^3}{12}\hat{B}\eta, \tag{32}$$

$$T = \int \left(\sigma_{13}^1 x_2 - \sigma_{12}^1 x_3\right) dA = -b\hat{D}\varepsilon_{11}^0 + \frac{b^3}{12}\hat{B}\mathrm{X}_{22} - b\hat{G}\mathrm{X}_{33} + \left(\frac{b^3}{12}\hat{H} + b\hat{M}\right)\eta, \tag{33}$$

where

$$\hat{B} = \sum_{k=1}^{n} \overline{Q}_{15}(h_k - h_{k-1}); \quad \hat{F} = \tfrac{1}{3}\sum_{k=1}^{n} \overline{Q}_{11}(h_k^3 - h_{k-1}^3); \quad \hat{G} = \tfrac{1}{3}\sum_{k=1}^{n} \overline{Q}_{16}(h_k^3 - h_{k-1}^3)$$
$$\hat{H} = \sum_{k=1}^{n} \overline{Q}_{55}(h_k - h_{k-1}); \quad \hat{M} = \tfrac{1}{3}\sum_{k=1}^{n} \overline{Q}_{66}(h_k^3 - h_{k-1}^3). \tag{34}$$

The generalized nodal forces can then be written in matrix form as

$$\mathbf{S} = \mathbf{DE}, \tag{35}$$

$$\mathbf{S} = \begin{Bmatrix} S_1 \\ S_2 \\ S_3 \\ S_4 \end{Bmatrix} = \begin{Bmatrix} N_{11} \\ M_{22} \\ M_{33} \\ T \end{Bmatrix}; \quad \mathbf{E} = \begin{Bmatrix} E_1 \\ E_2 \\ E_3 \\ E_4 \end{Bmatrix} = \begin{Bmatrix} \varepsilon_{11}^0 \\ \mathrm{X}_{22} \\ \mathrm{X}_{33} \\ \eta \end{Bmatrix}; \quad \mathbf{D} = b\begin{bmatrix} \hat{A} & 0 & \hat{C} & -\hat{D} \\ 0 & \frac{b^2}{12}\hat{A} & 0 & \frac{b^2}{12}\hat{B} \\ \hat{C} & 0 & \hat{F} & -\hat{G} \\ -\hat{D} & \frac{b^2}{12}\hat{B} & -\hat{G} & \frac{b^2}{12}\hat{H} + \hat{M} \end{bmatrix} \tag{36}$$

Now define the generalized displacement vector as

$$\mathbf{U} = \begin{Bmatrix} \hat{u}_1 \\ \hat{u}_2 \\ \hat{u}_3 \\ \hat{u}_4 \end{Bmatrix} = \begin{Bmatrix} u_{10} \\ u_{20} \\ u_{30} \\ \tau \end{Bmatrix}. \tag{37}$$

The generalized strain vector can be expressed as linear and nonlinear components

$$\mathbf{E} = \mathbf{E}^L + \mathbf{E}^N = \mathbf{LU} + \frac{1}{2}(\mathbf{AHU}), \tag{38}$$

where

$$\mathbf{L} = \begin{bmatrix} \frac{\partial}{\partial x_1} & 0 & 0 & 0 \\ 0 & -\frac{\partial^2}{\partial x_1^2} & 0 & 0 \\ 0 & 0 & -\frac{\partial^2}{\partial x_1^2} & 0 \\ 0 & 0 & 0 & \frac{\partial}{\partial x_1} \end{bmatrix}; \quad \mathbf{H} = \begin{bmatrix} 0 & 0 & 0 & 0 \\ 0 & 1 & 0 & 0 \\ 0 & 0 & 1 & 0 \\ 0 & 0 & 0 & 0 \end{bmatrix}\frac{\partial}{\partial x_1}; \quad \mathbf{A} = \begin{bmatrix} 0 & \frac{\partial \hat{u}_2}{\partial x_1} & \frac{\partial \hat{u}_3}{\partial x_1} & 0 \\ 0 & 0 & 0 & 0 \\ 0 & 0 & 0 & 0 \\ 0 & 0 & 0 & 0 \end{bmatrix}. \tag{39}$$

The element generalized mechanical stress vector can be written as

$$\mathbf{S}^{Mech} = \mathbf{DE}^L + \mathbf{DE}^N = \mathbf{S}^L + \mathbf{S}^N \tag{40}$$

3.3. Hygrothermal effects

The global coefficients of thermal expansion in a single lamina are related to the local ones through the transformation matrix as follows:

$$\boldsymbol{\alpha}_G = \mathbf{T}^{-1}\boldsymbol{\alpha}_L, \tag{41}$$

where $\boldsymbol{\alpha}_G = \left[\alpha_{11} \;\; \alpha_{22} \;\; \alpha_{33} \;\; \frac{\alpha_{23}}{2} \;\; \frac{\alpha_{31}}{2} \;\; \frac{\alpha_{12}}{2}\right]^T$; $\boldsymbol{\alpha}_L = \left[\alpha_{x'x'} \;\; \alpha_{y'y'} \;\; \alpha_{z'z'} \;\; 0 \;\; 0 \;\; 0\right]^T$.

The thermal stresses in a single lamina due to a temperature change (ΔT) can then be written as

$$\begin{Bmatrix} \sigma_{11}^{Th} \\ \sigma_{22}^{Th} \\ \sigma_{33}^{Th} \\ \sigma_{23}^{Th} \\ \sigma_{31}^{Th} \\ \sigma_{12}^{Th} \end{Bmatrix} = \overline{\mathbf{Q}}\begin{Bmatrix} \alpha_{11} \\ \alpha_{22} \\ \alpha_{33} \\ \alpha_{23} \\ \alpha_{31} \\ \alpha_{12} \end{Bmatrix}\Delta T. \tag{42}$$

By neglecting σ_{22}^{Th}, σ_{33}^{Th} and σ_{23}^{Th} as was done before, we get

$$\begin{Bmatrix} \sigma_{11}^{Th} \\ \sigma_{31}^{Th} \\ \sigma_{12}^{Th} \end{Bmatrix} = \begin{bmatrix} \overline{Q}_{11} & \overline{Q}_{15} & \overline{Q}_{16} \\ \overline{Q}_{51} & \overline{Q}_{55} & \overline{Q}_{56} \\ \overline{Q}_{61} & \overline{Q}_{56} & \overline{Q}_{66} \end{bmatrix}\begin{Bmatrix} \alpha_{11} \\ \alpha_{31} \\ \alpha_{12} \end{Bmatrix}\Delta T. \tag{43}$$

The nodal axial thermal force in x_1 direction can be expressed as

$$N_{11}^{Th} = \int_A \sigma_{11}^{Th} dA = \Delta T \int_A [\overline{Q}_{11}\alpha_{11} + \overline{Q}_{15}\alpha_{31} + \overline{Q}_{16}\alpha_{12}] dA = b\Delta T \int_{h_{k-1}}^{h_k} [\overline{Q}_{11}\alpha_{11} + \overline{Q}_{15}\alpha_{31} + \overline{Q}_{16}\alpha_{12}] dx_3 = b\Delta T\hat{N}, \tag{44}$$

where

$$\hat{N} = \sum_{k=1}^{n} [\overline{Q}_{11}\alpha_{11} + \overline{Q}_{15}\alpha_{31} + \overline{Q}_{16}\alpha_{12}](h_k - h_{k-1}) \tag{45}$$

The nodal bending moments about x_2 and x_3 (M_{33}^{Th} and M_{22}^{Th}) and the total torque about x_1 (T^{Th}) due to temperature change are derived similarly to get

$$M_{33}^{Th} = \int_A \sigma_{11}^{Th} x_3 dA = b\Delta T \int_{h_{k-1}}^{h_k} [\overline{Q}_{11}\alpha_{11} + \overline{Q}_{15}\alpha_{31} + \overline{Q}_{16}\alpha_{12}] x_3 dx_3 = b\Delta T\hat{O}, \tag{46}$$

$$M_{22}^{Th} = \int_A \sigma_{11}^{Th} x_2 dA = \Delta T \int_A [\overline{Q}_{11}\alpha_{11} + \overline{Q}_{15}\alpha_{31} + \overline{Q}_{16}\alpha_{12}] x_2 dA = 0, \tag{47}$$

$$T^{Th} = \int (\sigma_{13}^{Th} x_2 - \sigma_{12}^{Th} x_3) = -b\Delta T \int_{h_{k-1}}^{h_k} [\overline{Q}_{61}\alpha_{11} + \overline{Q}_{65}\alpha_{31} + \overline{Q}_{66}\alpha_{12}] x_3 dx_3 = -b\Delta T\hat{P}, \tag{48}$$

where

$$\hat{O} = \frac{1}{2}\sum_{k=1}^{n} [\overline{Q}_{11}\alpha_{11} + \overline{Q}_{15}\alpha_{31} + \overline{Q}_{16}\alpha_{12}](h_k^2 - h_{k-1}^2); \quad \hat{P} = \frac{1}{2}\sum_{k=1}^{n} [\overline{Q}_{61}\alpha_{11} + \overline{Q}_{65}\alpha_{31} + \overline{Q}_{66}\alpha_{12}](h_k^2 - h_{k-1}^2). \tag{49}$$

The generalized nodal forces due to temperature change can then be written in matrix form as

$$\mathbf{S}^{Th} = \begin{Bmatrix} S_1^{Th} \\ S_2^{Th} \\ S_3^{Th} \\ S_4^{Th} \end{Bmatrix} = \begin{Bmatrix} N_{11}^{Th} \\ M_{22}^{Th} \\ M_{33}^{Th} \\ T^{Th} \end{Bmatrix} = b\Delta T\begin{Bmatrix} \hat{N} \\ 0 \\ \hat{O} \\ -\hat{P} \end{Bmatrix} \tag{50}$$

Following the same process, the generalized nodal forces due to moisture absorption can be derived as

$$\mathbf{S}^{Moist} = \begin{Bmatrix} S_1^{Moist} \\ S_2^{Moist} \\ S_3^{Moist} \\ S_4^{Moist} \end{Bmatrix} = \begin{Bmatrix} N_{11}^{Moist} \\ M_{22}^{Moist} \\ M_{33}^{Moist} \\ T^{Moist} \end{Bmatrix} = b\Delta C \begin{Bmatrix} \hat{R} \\ 0 \\ \hat{W} \\ -\hat{X} \end{Bmatrix}, \tag{51}$$

where

$$\begin{aligned} \hat{R} &= \sum_{k=1}^{n} [\overline{Q}_{11}\beta_{11} + \overline{Q}_{15}\beta_{31} + \overline{Q}_{16}\beta_{12}](h_k - h_{k-1}); \quad \hat{W} \\ &= \tfrac{1}{2}\sum_{k=1}^{n} [\overline{Q}_{11}\beta_{11} + \overline{Q}_{15}\beta_{31} + \overline{Q}_{16}\beta_{12}](h_k^2 - h_{k-1}^2) \\ \hat{X} &= \tfrac{1}{2}\sum_{k=1}^{n} [\overline{Q}_{61}\beta_{11} + \overline{Q}_{65}\beta_{31} + \overline{Q}_{66}\beta_{12}](h_k^2 - h_{k-1}^2) \end{aligned} \tag{52}$$

β_{ij} are the moisture expansion coefficients, and ΔC is the change in the weight of moisture absorbed per unit weight of the lamina. The hygrothermal generalized nodal forces $\mathbf{S}^{Th}$ and $\mathbf{S}^{Moist}$ are added to the mechanical generalized nodal forces $\mathbf{S}^{Mech}$ in Eq. (40).

4. Updated Lagrangian formulation in the co-rotational reference frame

4.1. Interpolation functions

The generalized displacement vector in a beam element with two nodes and six degrees of freedom per node can be expressed as [30]

$$\mathbf{U} = \mathbf{N}\hat{\mathbf{a}} = [\mathbf{N_1} \quad \mathbf{N_2}] \begin{Bmatrix} \mathbf{u}^1 \\ \mathbf{u}^2 \end{Bmatrix}, \tag{53}$$

where $\mathbf{N}_i$ contains the shape functions

$$\mathbf{N_1} = \begin{bmatrix} \phi_1 & 0 & 0 & 0 & 0 & 0 \\ 0 & N_1 & 0 & 0 & 0 & N_2 \\ 0 & 0 & N_1 & 0 & -N_2 & 0 \\ 0 & 0 & 0 & \phi_1 & 0 & 0 \end{bmatrix}; \quad \mathbf{N_2} = \begin{bmatrix} \phi_2 & 0 & 0 & 0 & 0 & 0 \\ 0 & N_3 & 0 & 0 & 0 & N_4 \\ 0 & 0 & N_3 & 0 & -N_4 & 0 \\ 0 & 0 & 0 & \phi_2 & 0 & 0 \end{bmatrix} \tag{54}$$

$$\begin{aligned} &\phi_1 = 1-\xi; \quad \phi_2 = \xi \\ &N_1 = 1-3\xi^2 + 2\xi^3; \quad N_2 = (\xi - 2\xi^2 + \xi^3)l; \quad N_3 = 3\xi^2 - 2\xi^3; \quad N_4 \\ &= (\xi^3 - \xi^2)l \end{aligned} \tag{55}$$

l is the length of the beam element, and ξ is the non-dimensional coordinate,

$$\xi = \frac{x_1 - x_1^1}{l}, \quad (0 < \xi < 1), \tag{56}$$

and x_1^1 is the coordinate of first node along x_1.

$\mathbf{u}^i$ is the nodal degrees of freedom vector at node i in the UL co-rotational frame e_i in Fig. 1 (left):

$$\mathbf{u}^i = [u_1^i \;\; u_2^i \;\; u_3^i \;\; u_4^i \;\; u_5^i \;\; u_6^i]^T = [u_{10}^i \;\; u_{20}^i \;\; u_{30}^i \;\; \tau^i \;\; \eta_{20}^i \;\; \eta_{30}^i]^T, \quad [i = 1,2] \tag{57}$$

where η_{20}^i and η_{30}^i are the nodal slopes in the 1–3 and 1–2 planes respectively as shown in Fig. 1 (left).

The element generalized strains can be rewritten as

$$\mathbf{E} = \mathbf{E}^L + \mathbf{E}^N = (\mathbf{B}^L + \hat{\mathbf{B}}^N)\hat{\mathbf{a}}, \tag{58}$$

where

$$\mathbf{B}^L = \begin{bmatrix} \frac{\partial\phi_1}{\partial x_1} & 0 & 0 & 0 & 0 & 0 \\ 0 & -\frac{\partial^2 N_1}{\partial x_1^2} & 0 & 0 & 0 & -\frac{\partial^2 N_2}{\partial x_1^2} \\ 0 & 0 & -\frac{\partial^2 N_1}{\partial x_1^2} & 0 & \frac{\partial^2 N_2}{\partial x_1^2} & 0 \\ 0 & 0 & 0 & \frac{\partial\phi_1}{\partial x_1} & 0 & 0 \\ \frac{\partial\phi_2}{\partial x_1} & 0 & 0 & 0 & 0 & 0 \\ 0 & -\frac{\partial^2 N_3}{\partial x_1^2} & 0 & 0 & 0 & -\frac{\partial^2 N_4}{\partial x_1^2} \\ 0 & 0 & -\frac{\partial^2 N_3}{\partial x_1^2} & 0 & \frac{\partial^2 N_4}{\partial x_1^2} & 0 \\ 0 & 0 & 0 & \frac{\partial\phi_2}{\partial x_1} & 0 & 0 \end{bmatrix} \tag{59}$$

$$\hat{\mathbf{B}}^N = \frac{1}{2}\mathbf{AHN} = \frac{1}{2}\begin{bmatrix} 0 & \frac{\partial N_1}{\partial x_1}\frac{\partial \hat{u}_2^i}{\partial x_1} & \frac{\partial N_1}{\partial x_1}\frac{\partial \hat{u}_3^i}{\partial x_1} & 0 & -\frac{\partial N_2}{\partial x_1}\frac{\partial \hat{u}_3^i}{\partial x_1} & \frac{\partial N_2}{\partial x_1}\frac{\partial \hat{u}_2^i}{\partial x_1} \\ 0 & 0 & 0 & 0 & 0 & 0 \\ 0 & 0 & 0 & 0 & 0 & 0 \\ 0 & 0 & 0 & 0 & 0 & 0 \\ 0 & \frac{\partial N_3}{\partial x_1}\frac{\partial \hat{u}_2^i}{\partial x_1} & \frac{\partial N_3}{\partial x_1}\frac{\partial \hat{u}_3^i}{\partial x_1} & 0 & -\frac{\partial N_4}{\partial x_1}\frac{\partial \hat{u}_3^i}{\partial x_1} & \frac{\partial N_4}{\partial x_1}\frac{\partial \hat{u}_2^i}{\partial x_1} \\ 0 & 0 & 0 & 0 & 0 & 0 \\ 0 & 0 & 0 & 0 & 0 & 0 \\ 0 & 0 & 0 & 0 & 0 & 0 \end{bmatrix} \tag{60}$$

Therefore

$$\delta\mathbf{E} = (\mathbf{B}^L + 2\hat{\mathbf{B}}^N)\delta\hat{\mathbf{a}} = (\mathbf{B}^L + \mathbf{B}^N)\delta\hat{\mathbf{a}}, \tag{61}$$

where δ indicates the variation.

4.2. Weak formulation of the beam element in the co-rotational reference frame

The stress tensor is equal to the initial Cauchy stress, τ_{ik}^0, plus the incremental Piola-Kirchhoff stress, σ_{ik}^1, in the UL co-rotational frame

$$\sigma_{ik} = \sigma_{ik}^1 + \tau_{ik}^0. \tag{62}$$

The equilibrium static equation and boundary conditions in the composite beam can be written as

$$\frac{\partial}{\partial x_i}\left[(\sigma_{ik}^1 + \tau_{ik}^0)\left(\delta_{jk} + \frac{\partial u_j}{\partial x_k}\right)\right] + b_j = 0, \tag{63}$$

$$(\sigma_{ik}^1 + \tau_{ik}^0)\left(\delta_{jk} + \frac{\partial u_j}{\partial x_k}\right)n_i - f_i = 0, \tag{64}$$

where b_j are the body forces per unit volume in the current reference state, and f_j are the given boundary loads.

By taking δu_j to be the test function, the weak form of Eqs. (63) and (64) can be expressed as

$$\int_V \left\{\frac{\partial}{\partial x_i}\left[\sigma_{ik}\left(\delta_{jk} + \frac{\partial u_j}{\partial x_k}\right)\right] + b_j\right\}\delta u_j dV - \int_{S_\sigma}\left[\sigma_{ik}\left(\delta_{jk} + \frac{\partial u_j}{\partial x_k}\right)n_i - f_i\right]\delta u_j dS = 0, \tag{65}$$

where n_i is the outward unit normal to the boundary surface S_σ.

By using the Divergence theorem and integration by parts, Eq. (65) can be written as

$$\int_V -\sigma_{ik}\left(\delta_{jk} + \frac{\partial u_j}{\partial x_k}\right)\delta u_{j,i} dV + \int_V b_j \delta u_j dV + \int_{S_\sigma} f_j \delta u_j dS = 0 \tag{66}$$

Using Eq. (24), the incremental Piola-Kirchhoff stress can be written as

Table 1
Mechanical properties of *Mat-A*, and *Mat-B*.

Mechanical properties	*Mat-A*	*Mat-B*	Unit
$E_{x'}$	181	204	GPa
$E_{y'}$	10.3	18.5	GPa
$E_{z'}$	10.3	18.5	GPa
$\nu_{x'y'}$	0.28	0.23	–
$\nu_{y'z'}$	0.4	0.4	–
$\nu_{x'z'}$	0.28	0.23	–
$G_{x'y'}$	7.17	5.59	GPa
$G_{y'z'}$	3.67	7.52	GPa
$G_{z'x'}$	7.17	5.59	GPa
$\alpha_{x'}$	0.02	6.1	μm/m/°C
$\alpha_{y'}$	22.5	30.3	μm/m/°C
$\alpha_{z'}$	22.5	30.3	μm/m/°C
$\beta_{x'}$	0	0	m/m/kg/kg
$\beta_{y'}$	0.6	0.6	m/m/kg/kg
$\beta_{z'}$	0.6	0.6	m/m/kg/kg

$$\sigma_{ik}^{1} = \sigma_{ik}^{1L} + \sigma_{ik}^{1N} \tag{67}$$

Therefore the first term of Eq. (66) could be developed as

$$\begin{aligned}\sigma_{ik}(\delta_{jk} + u_{j,k})\delta u_{j,i} &= (\tau_{ij}^{0} + \tau_{ik}^{0}u_{j,k} + \sigma_{ij}^{1L} + \sigma_{ij}^{1N} + \sigma_{ik}^{1}u_{j,k})\delta u_{j,i} \\ &= \sigma_{ij}^{1L}\delta u_{i,j} + (\tau_{ij}^{0} + \sigma_{ij}^{1N})\delta u_{j,i} + \tau_{ik}^{0}\delta\left(\frac{1}{2}u_{j,k}u_{j,i}\right) \\ &\quad + \sigma_{ik}^{1}\delta\left(\frac{1}{2}u_{j,k}u_{j,i}\right),\end{aligned} \tag{68}$$

where we used $\delta\left(\frac{1}{2}u_{j,k}u_{j,i}\right) = \frac{1}{2}(u_{j,k}\delta u_{j,i} + u_{j,i}\delta u_{j,k}) = u_{j,k}\delta u_{j,i}$ since $u_{i,j} = u_{j,i}$.

Using Eq. (68), and the definitions $\varepsilon_{ij}^{L} = u_{i,j}$, $\varepsilon_{ij}^{N} = \frac{1}{2}u_{k,i}u_{k,j}$, Eq. (66) can be written as

$$\begin{aligned}\int_V (\sigma_{ij}^{1L}\delta\varepsilon_{ij}^{L} + \tau_{ij}^{0}\delta\varepsilon_{ij}^{N})dV &= \int_V b_j\delta u_j dV + \int_{S_\sigma} f_j\delta u_j dS \\ &\quad - \int_V [(\sigma_{ij}^{1N} + \tau_{ij}^{0})\delta\varepsilon_{ij}^{L} + \sigma_{ij}^{1}\delta\varepsilon_{ij}^{N}]dV.\end{aligned} \tag{69}$$

The right-hand side of Eq. (69) is the "correction" term in Newton-Rapson type iterative approach. By assuming the cross sectional area of the composite beam to be constant along x_1-direction, and by using Eqs. (55)–(61), the integration terms in the above equation could be expressed as

$$\sum_{e=1}^{N_e}\left[\delta\hat{\mathbf{a}}^T\int_l (\mathbf{B}^L)^T\mathbf{D}\mathbf{B}^L dl\hat{\mathbf{a}} + \delta\hat{\mathbf{a}}^T\int_l (\mathbf{B}^N)^T\boldsymbol{\tau}^0 dl\right] = \sum_{e=1}^{N_e}[\delta\hat{\mathbf{a}}^T\hat{\mathbf{F}}^1 - \delta\hat{\mathbf{a}}^T\int_l (\mathbf{B}^L)^T(\boldsymbol{\tau}^0 + \boldsymbol{\sigma}^{1N})dl - \delta\hat{\mathbf{a}}^T\int_l (\mathbf{B}^N)^T\boldsymbol{\sigma}^1 dl], \tag{70}$$

where the summation is taken over all finite elements N_e, and $\hat{\mathbf{F}}^1$ is the external equivalent nodal force vector,

$$\hat{\mathbf{F}}^1 = \int_l \mathbf{N}^T\mathbf{b}^* dl + \mathbf{f}^*, \tag{71}$$

where $\mathbf{b}^*$ is the external body force vector per unit volume, and $\mathbf{f}^*$ is the external nodal boundary traction vector.

Eq. (70) can be rewritten as:

$$\sum_e [\delta\hat{\mathbf{a}}^T(\hat{\mathbf{K}})\hat{\mathbf{a}}] = \sum_e [\delta\hat{\mathbf{a}}^T(\hat{\mathbf{F}}^1 - \hat{\mathbf{F}}^S)], \tag{72}$$

where $\hat{\mathbf{K}}$ the symmetric stiffness matrix of the laminated composite beam and is expressed as

$$\hat{\mathbf{K}} = \hat{\mathbf{K}}^L + \hat{\mathbf{K}}^N. \tag{73}$$

The linear and nonlinear parts of the stiffness matrix are

$$\hat{\mathbf{K}}^L = \int_l (\mathbf{B}^L)^T\mathbf{D}\mathbf{B}^L dl, \quad \hat{\mathbf{K}}^N = \int_l \tau_1^0\mathbf{G}^T\mathbf{G}dl, \tag{74}$$

where we used the fact that $\int_l (\mathbf{B}^N)^T\boldsymbol{\tau}^0 dl = (\int_l \tau_1^0\mathbf{G}^T\mathbf{G}dl)\hat{\mathbf{a}} = \hat{\mathbf{K}}^N\hat{\mathbf{a}}$, where τ_1^0 is the first term of the initial Cauchy stress. $\hat{\mathbf{F}}^S$ is the internal nodal force,

$$\hat{\mathbf{F}}^S = \int_l (\mathbf{B}^L)^T(\boldsymbol{\tau}^0 + \boldsymbol{\sigma}^{1N})dl + \int_l (\mathbf{B}^N)^T\boldsymbol{\sigma}^1 dl. \tag{75}$$

By neglecting the nonlinear terms in the above equation, $\hat{\mathbf{F}}^S$ can be simplified as

$$\hat{\mathbf{F}}^S = \int_l (\mathbf{B}^L)^T\boldsymbol{\tau}^0 dl = l\int_0^1 (\mathbf{B}^L)^T\boldsymbol{\tau}^0 d\xi. \tag{76}$$

The initial Cauchy stress in Eq. (76) can be written as

$$\boldsymbol{\tau}^0 = \mathbf{S}^{Mech,0} - \mathbf{S}^{Th} - \mathbf{S}^{Moist} \tag{77}$$

Therefore Eq. (76) can be expanded as

$$\hat{\mathbf{F}}^S = l\int_0^1 (\mathbf{B}^L)^T\mathbf{S}^{Mech,0}d\xi - l\int_0^1 (\mathbf{B}^L)^T\mathbf{S}^{Th}d\xi - l\int_0^1 (\mathbf{B}^L)^T\mathbf{S}^{Moist}d\xi \tag{78}$$

4.3. Explicit expressions for the tangent stiffness matrix

The integration in Eq. (74) can be evaluated, and the 12×12 nonlinear stiffness matrix can be simplified as

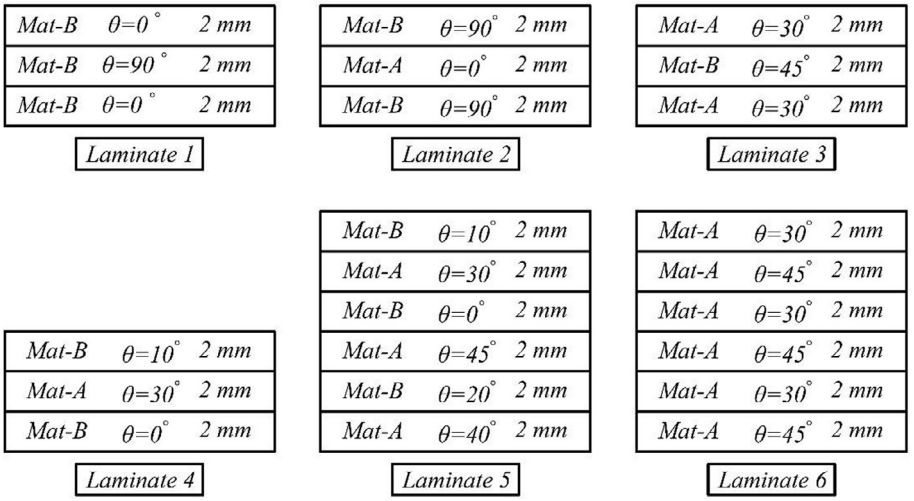

Fig. 3. Six different laminates used in the simulations.

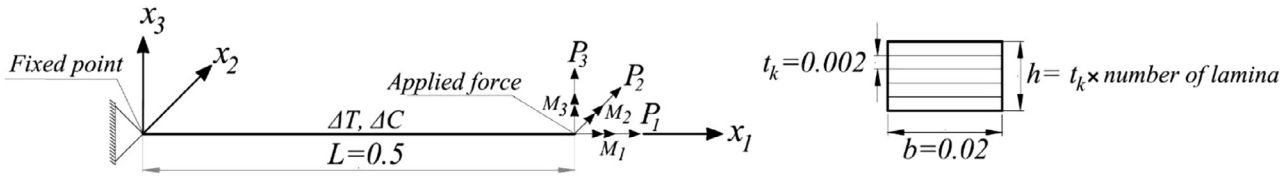

Fig. 4. Cantilever beam subjected to forces and moments in different directions at its tip.

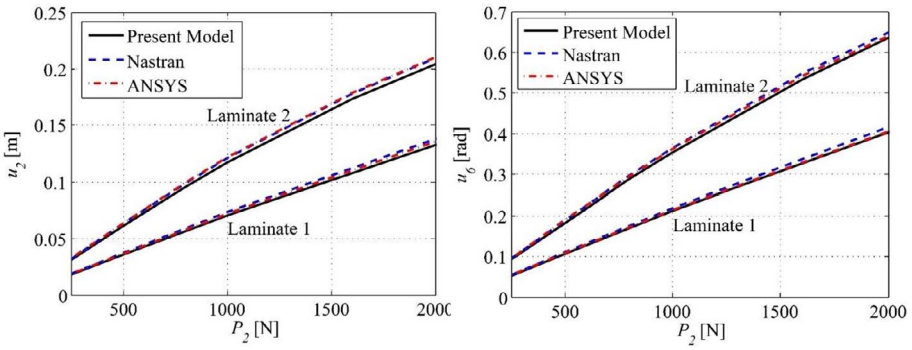

Fig. 5. (left) u_2 displacement, (right) u_6 rotation vs. P_2 tip force on the laminated composite cantilever beam.

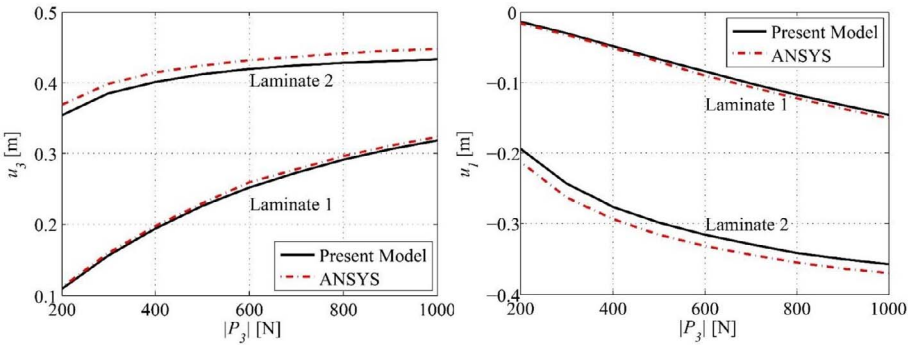

Fig. 6. (left) u_3, (right) u_1 displacements vs. P_3 tip force on the laminated composite cantilever beam.

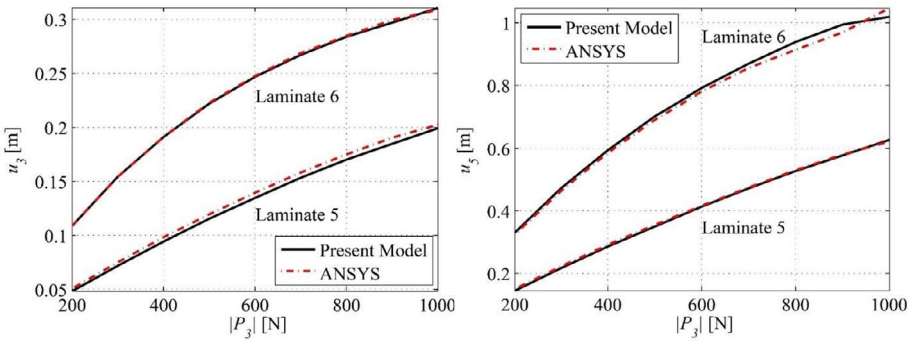

Fig. 7. (left) u_3 displacement, (right) u_5 rotation vs. P_3 tip force on the laminated composite cantilever beam.

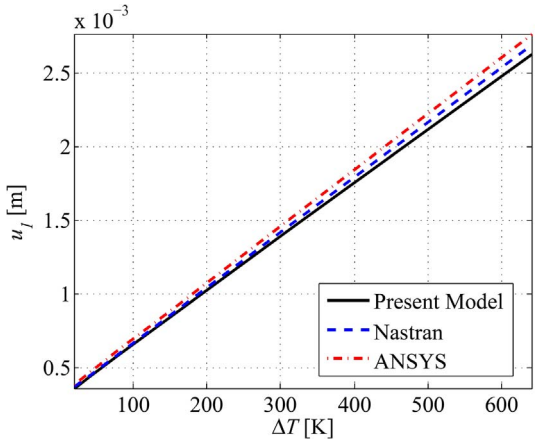

Fig. 8. u_1 displacement vs. ΔT with constant tip force $P_1 = 10{,}000$ N on the laminated composite cantilever beam (Laminate 1 cross section).

$$\hat{\mathbf{K}}^N = \tau_1^0 \begin{bmatrix} 0 & 0 & 0 & 0 & 0 & 0 & 0 & 0 & 0 & 0 & 0 & 0 \\ & a & 0 & 0 & 0 & 0.1 & 0 & -a & 0 & 0 & 0 & 0.1 \\ & & a & 0 & -0.1 & 0 & 0 & 0 & -a & 0 & -0.1 & 0 \\ & & & 0 & 0 & 0 & 0 & 0 & 0 & 0 & 0 & 0 \\ & & & & c & 0 & 0 & 0 & 0.1 & 0 & -d & 0 \\ & & & & & c & 0 & -0.1 & 0 & 0 & 0 & -d \\ & & & & & & 0 & 0 & 0 & 0 & 0 & 0 \\ & & & & & & & a & 0 & 0 & 0 & -0.1 \\ & & sym. & & & & & & a & 0 & 0.1 & 0 \\ & & & & & & & & & 0 & 0 & 0 \\ & & & & & & & & & & c & 0 \\ & & & & & & & & & & & c \end{bmatrix} \tag{79}$$

where $a = \frac{1.2}{l}$; $c = \frac{2l}{15}$; $d = \frac{l}{30}$ and l is the current length of the beam in the current local reference frame. Again, the width of the laminated composite beam, b, is assumed to be constant, and the integration in Eq. (74) can be evaluated. The 12×12 linear stiffness matrix can be expressed as

$$\hat{\mathbf{K}}^L = \frac{b}{l}\begin{bmatrix} \hat{\mathbf{K}}_1^L & \hat{\mathbf{K}}_2^L \\ (\hat{\mathbf{K}}_2^L)^T & \hat{\mathbf{K}}_3^L \end{bmatrix} \tag{80}$$

where

$$\hat{\mathbf{K}}_1^L = \begin{bmatrix} \hat{A} & 0 & 0 & -\hat{D} & \hat{C} & 0 \\ & \frac{b^2}{l^2}\hat{A} & 0 & 0 & 0 & \frac{b^2}{2l}\hat{A} \\ & & \frac{12}{l^2}\hat{F} & 0 & -\frac{6}{l}\hat{F} & 0 \\ & & & \frac{b^2}{12}\hat{H} + \hat{M} & -\hat{G} & -\frac{b^2}{12}\hat{B} \\ & sym. & & & 4\hat{F} & 0 \\ & & & & & \frac{b^2}{3}\hat{A} \end{bmatrix} \tag{81}$$

$$\hat{\mathbf{K}}_2^L = \begin{bmatrix} -\hat{A} & 0 & 0 & \hat{D} & -\hat{C} & 0 \\ 0 & -\frac{b^2}{l^2}\hat{A} & 0 & 0 & 0 & \frac{b^2}{2l}\hat{A} \\ 0 & 0 & -\frac{12}{l^2}\hat{F} & 0 & -\frac{6}{l}\hat{F} & 0 \\ \hat{D} & 0 & 0 & -\frac{b^2}{12}\hat{H} - \hat{M} & \hat{G} & \frac{b^2}{12}\hat{B} \\ -\hat{C} & 0 & \frac{6}{l}\hat{F} & \hat{G} & 2\hat{F} & 0 \\ 0 & -\frac{b^2}{2l}\hat{A} & 0 & \frac{b^2}{12}\hat{B} & 0 & \frac{b^2}{6}\hat{A} \end{bmatrix} \tag{82}$$

$$\hat{\mathbf{K}}_3^L = \begin{bmatrix} \hat{A} & 0 & 0 & -\hat{D} & \hat{C} & 0 \\ & \frac{b^2}{l^2}\hat{A} & 0 & 0 & 0 & -\frac{b^2}{2l}\hat{A} \\ & & \frac{12}{l^2}\hat{F} & 0 & \frac{6}{l}\hat{F} & 0 \\ & & & \frac{b^2}{12}\hat{H} + \hat{M} & -\hat{G} & -\frac{b^2}{12}\hat{B} \\ & sym. & & & 4\hat{F} & 0 \\ & & & & & \frac{b^2}{3}\hat{A} \end{bmatrix} \tag{83}$$

The 12×12 transformation matrix between the generalized local coordinates of the deformed configuration of the composite beam element and the global coordinates can be written in terms of $\boldsymbol{\lambda}_0$ given in Eq. (9) as

$$\boldsymbol{\lambda} = \begin{bmatrix} \boldsymbol{\lambda}_0 & \mathbf{0} & \mathbf{0} & \mathbf{0} \\ \mathbf{0} & \boldsymbol{\lambda}_0 & \mathbf{0} & \mathbf{0} \\ \mathbf{0} & \mathbf{0} & \boldsymbol{\lambda}_0 & \mathbf{0} \\ \mathbf{0} & \mathbf{0} & \mathbf{0} & \boldsymbol{\lambda}_0 \end{bmatrix}, \quad \mathbf{0} = \begin{bmatrix} 0 & 0 & 0 \\ 0 & 0 & 0 \\ 0 & 0 & 0 \end{bmatrix}. \tag{84}$$

Therefore, the generalized nodal displacement vector, the element tangent stiffness matrix, and generalized nodal forces can be transferred from the local coordinates to the global coordination as

$$\tilde{\tilde{\mathbf{a}}}^k = \boldsymbol{\lambda}^T \hat{\mathbf{a}}^k; \quad \tilde{\tilde{\mathbf{K}}}^k = \boldsymbol{\lambda}^T \hat{\mathbf{K}}^k \boldsymbol{\lambda}; \quad \tilde{\tilde{\mathbf{F}}}^k = \boldsymbol{\lambda}^T \hat{\mathbf{F}}^k \tag{85}$$

Now, the stiffness matrix can be assembled, and the finite element system of equations can be expressed as:

$$\mathbf{K}\mathbf{a} = \mathbf{F}^{\mathrm{I}} - \mathbf{F}^{S0} \tag{86}$$

At this stage, the Newton-Raphson algorithm can be used to solve the above equation iteratively. The iterative process of the Newton-Raphson method can be written as

$$\mathbf{K}^{(m)}\mathbf{a}^{(m)} = \mathbf{F}^{\mathrm{I}} - \mathbf{F}^{S(m)} \tag{87}$$

where m is the iteration number and

$$\mathbf{F}^{S(m)} = l\int_0^1 (\mathbf{B}^L)^T \boldsymbol{\tau}^{0(m)} d\xi \tag{88}$$

The total displacements for all nodes can then be written as

$$\mathbf{u}^{(m+1)} = \mathbf{u}^{(m)} + \mathbf{a}^{(m)} \tag{89}$$

A Matlab code has been developed to implement the proposed formulation, and solve the system of equations iteratively with applied increments of the mechanical loads, until the total applied load is reached and a converged solution is obtained.

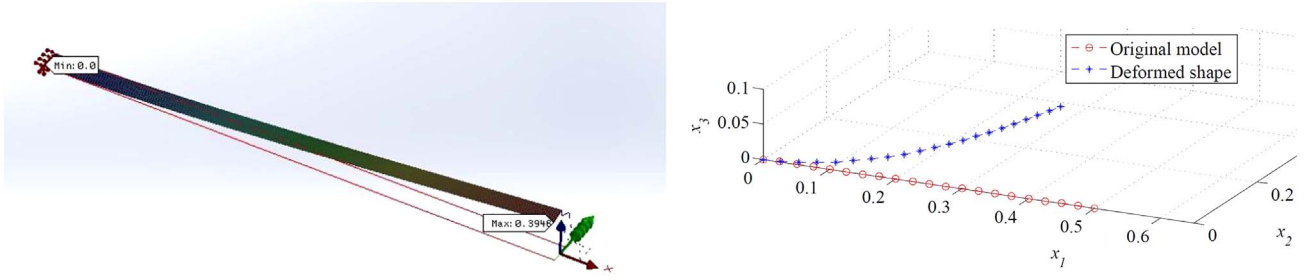

Fig. 9. Deformation of the laminated composite cantilever beam for the case of $P_2 = 16{,}000$ N, $\Delta T = 300$ K (Laminate 1 cross section): (left) Nastran, (right) Present model.

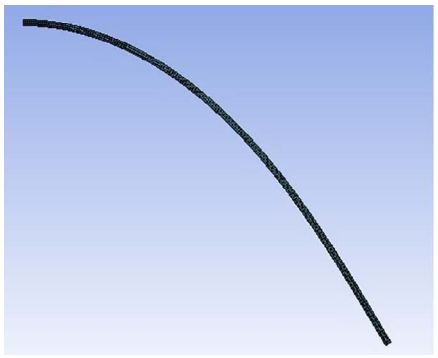

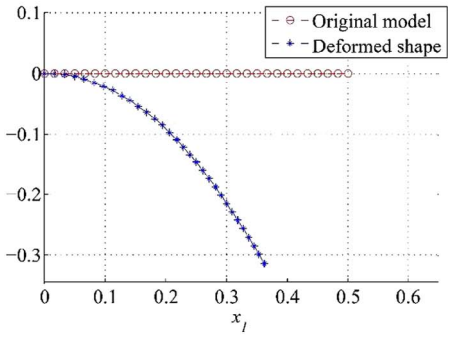

Fig. 10. Deformation of the laminated composite cantilever beam for the case of $P_3 = -1000$ N, $\Delta T = 300$ K (Laminate 1 cross section): (left) ANSYS and (right) Present model.

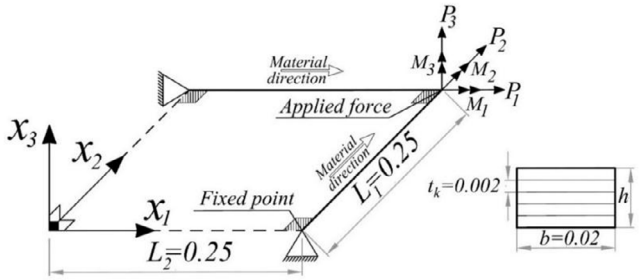

Fig. 11. L-shaped structure subjected to forces and moments.

5. Numerical examples

Several numerical examples are presented in this section to demonstrate the efficiency of the proposed method. The composite laminae used in this section are made of *Mat-A* and *Mat-B* whose properties are listed in Table 1. Six different composite laminates, illustrated in Fig. 3, are used to demonstrate different cases of stacking sequence, laminae materials, and symmetry.

Nastran-in-CAD finite element tool available with SolidWorks is used in the first two examples in this section for comparison with the results of the developed Matlab code for the proposed method. This tool has the option of using a laminated composite material given the stacking sequence and the material properties and thicknesses of all laminae. Laminates should be defined on a shell, not a solid or structural elements such as beams, and loads should be applied only in the plane of the shell. It was found that applying loads perpendicular to the plane of the laminate in Nastran (2016) always give unrealistic results as compared to ANSYS. This happens even if the full 3D material properties of the laminae are given (the nine material properties of orthotropic materials). Hence, in the following examples, we compare the results of the developed Matlab code with Nastran results only when the loads are applied in the plane of the composite laminate. We also compare with ANSYS finite element tool results when loads are applied perpendicular to the plane of the laminate. It is important to note that the proposed formulation is just modeling the laminated composite structures using 1D beam elements, while Nastran requires 2D plate elements and ANSYS requires 3D Solid elements to model composite laminates.

5.1. Large deformation analysis of a cantilever laminated composite beam

Consider a cantilever beam subjected to forces P_1, P_2, P_3 and moments M_1, M_2, M_3 at its tip, in addition to temperature and moisture change on the whole beam, as shown in Fig. 4. The beam is made of a fiber-reinforced composite laminate with a rectangular cross section, as shown in Fig. 3. The length of the beam is $L = 0.5$ m, its width is $b = 0.02$ m, and the thickness of each lamina is $t_s = 0.002$ m. The beam is analyzed for different cases of loadings using the developed Matlab code for the proposed method as well as using ANSYS and Nastran finite element packages.

To find the solution that best balances computational capacity and accuracy, convergence study has been performed for Nastran, ANSYS and the proposed method for the cantilever beam model. The convergence study on Nastran and ANSYS began with 22 2D square shell elements and 40 3D solid cube elements along x_1 direction respectively. The mesh density has been increased until convergence was reached with 225 2D shell elements along x_1 direction for Nastran model, 234 3D solid elements along x_1 direction for ANSYS model and 30 1D beam element along x_1 direction for the developed Matlab code. Total number of 2D elements in Nastran is 2030 corresponding to 2263 nodes, total number of 3D solid elements in ANSYS is 2361 corresponding to 2576 nodes and total number of 1D elements in Matlab is 30 corresponding to 31 nodes.

The results of the different applied mechanical and hygrothermal loads on beams made of a laminated fiber-reinforced composite with a rectangular cross section as shown in Fig. 4 are presented in Figs. 5–10 using the proposed method, Nastran and ANSYS. Specifically, Fig. 5

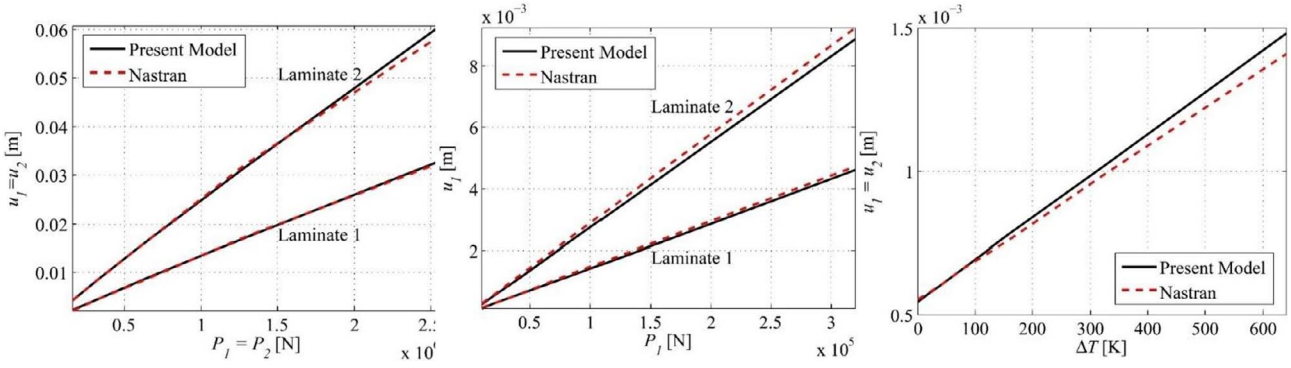

Fig. 12. Laminated composite L-shaped structure: (left) $u_1 = u_2$ displacements vs $P_1 = P_2$ tip forces, (middle) u_1 displacement vs P_1 tip force, (right) $u_1 = u_2$ vs ΔT with constant tip forces $P_1 = P_2 = 20{,}000$ N (Laminate 2).

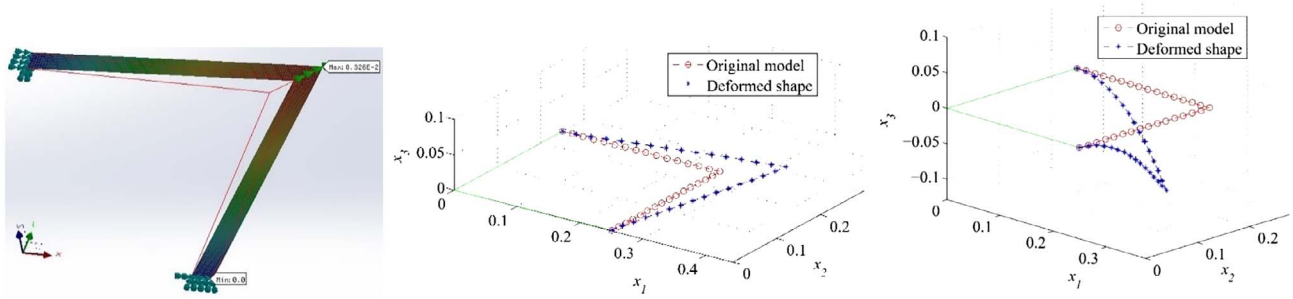

Fig. 13. Deformation of the laminated composite L-shaped structure with Laminate 1 cross section: (left) $P_1 = P_2 = 5{,}120{,}000$ N Nastran and (middle) Present model, (right) $P_3 = -10{,}000$ N.

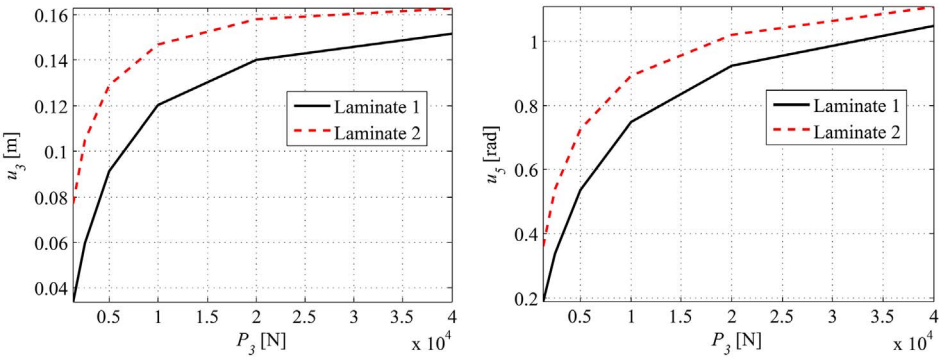

Fig. 14. (left) u_3 displacement, (right) u_5 rotation vs. P_3 tip force on the laminated composite L-shaped structure.

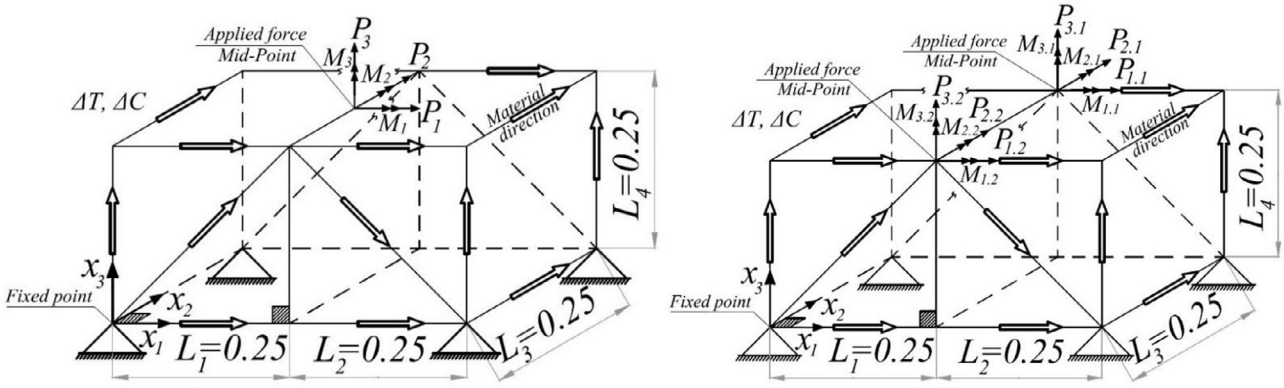

Fig. 15. 3D composite frame structure subjected to forces and moments in different directions (left) on a single point, (right) on two points.

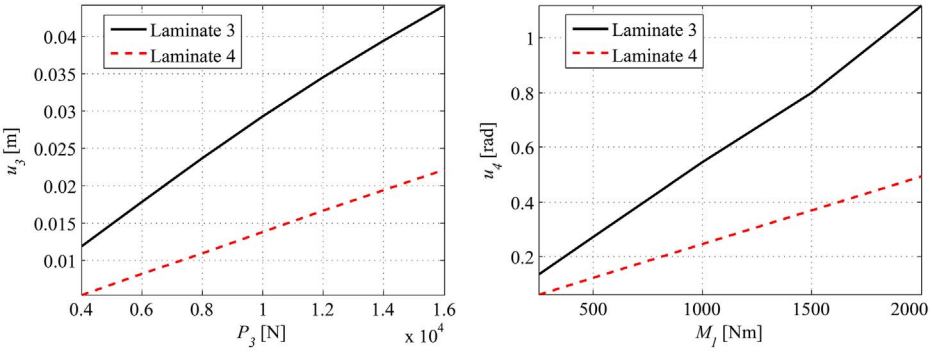

Fig. 16. (left) u_3 displacement vs P_3 force, (right) u_4 rotation vs M_1 moment on the mid point of the upper middle member of the laminated composite 3D frame.

shows u_2 and u_6 (rotation about x_3 axis) at the beam tip for increasing values of applied force P_2. Applying force P_3 at the tip of the composite beam, Fig. 6 shows u_3 and u_1 at the beam tip with Laminates 1 and 2 rectangular cross sections, while Fig. 7 shows u_3 and u_5 (rotation about x_2 axis) with Laminates 5 and 6 for increasing values of P_3. Fig. 8 shows the effect of temperature on u_1 with constant $P_1 = 10{,}000$ N applied force. Excellent agreement with Nastran and ANSYS can be seen in all cases. The maximum error percent is less than 5% in all cases. Fig. 9 shows the deformation of Nastran model and the proposed method with Laminate 1 cross section for the case of $P_2 = 16{,}000$ N, $\Delta T = 300$ K. For this specific case, Nastran takes 26 minutes and 5 seconds to find the solution, while the developed Matlab code takes only 1 minute and

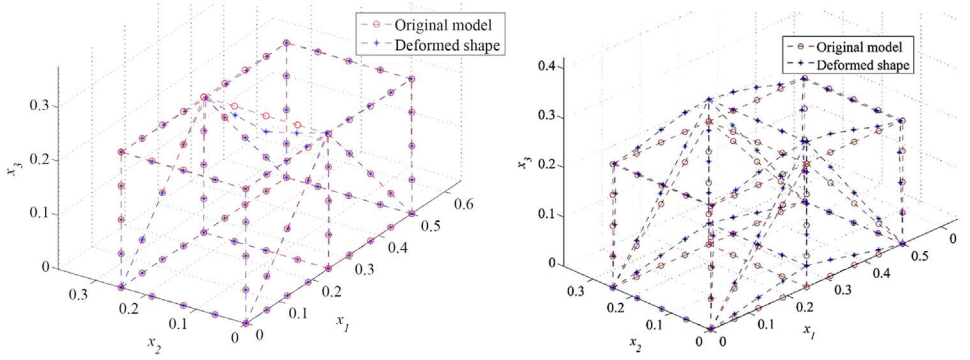

Fig. 17. Deformation of the laminated composite 3D frame structure subjected to (left) force $P_3 = -10{,}000$ N on the mid point of the upper middle member, (right) forces $P_{3.1} = P_{3.2} = 1{,}600{,}000$ N at the two ends of the upper middle member (Laminate 3 cross section).

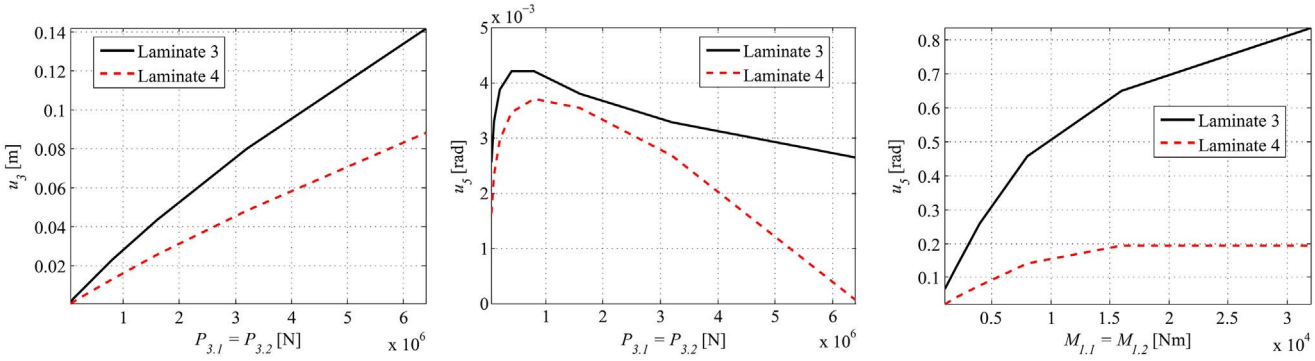

Fig. 18. (left) u_3 displacement, (middle) u_5 rotation vs $P_{3.1} = P_{3.2}$, (left) u_5 vs $M_{1.1} = M_{1.2}$ (with constant forces $P_{3.1} = P_{3.2} = 400{,}000$ N) applied on the two ends of the upper middle member of the laminated composite 3D frame.

39 seconds to solve the problem. This is 6.3% the time required by Nastran. Fig. 10 shows the deformation of ANSYS model and the proposed method with Laminate 1 rectangular cross section for the case of $P_3 = -1000$ N, $\Delta T = 300$ K. For this specific case, ANSYS takes 3 minutes and 37 seconds to find the solution, while the developed Matlab code takes only 44 seconds to solve the problem. This is 20.2% the time required by ANSYS.

5.2. Large deformation analysis of simply supported L-shape structure

In this example, an L-shaped structure is subjected to forces P_1, P_2, P_3 and moments M_1, M_2, M_3 at the illustrated point in Fig. 11 as well as changes in temperature and moisture content on the whole structure. This structure has two equal side lengths $L_1 = L_2 = 0.25$ m, and has two fixed points at its two ends. Each side of this structure is a laminated composite beam with a rectangular cross-section of width $b = 0.02$ m. The element size of both Matlab code and Nastran models are equal to the element size of the cantilever beam example. Accordingly, in this example, 30 1D beam elements (31 nodes) are used to model the structure using the developed method, while 2029 2D elements (216 2D shell elements along x_1 direction) corresponding to 6573 nodes are used to model the L-shaped structure in SolidWorks with Nastran-in-CAD tool.

The displacement of the load-application point in the laminated composite L-shaped structure made of two different composite laminates for the different applied mechanical and hygrothermal loads are presented in Fig. 12 for the present method and Nastran. Excellent agreement can be seen in all cases. Fig. 13 (left and middle) show the deformation of both Matlab code and Nastran models with Laminate 1 cross section for the case of $P_1 = P_2 = 5{,}120{,}000$ N. Fig. 14 shows the u_3 displacement of the load-application point when P_3 force is applied. As was mentioned earlier, Nastran (2016) provides unrealistic large deformations when the load is applied perpendicular to the plane of the laminate. Fig. 13 (right) shows the deformation of the same structure with $P_3 = -10{,}000$ N applied using the developed Matlab code.

5.3. Large deformation analysis of a composite 3D frame

In this example, a 3D frame structure, shown in Fig. 15, is subjected to forces P_1, P_2, P_3 and moments M_1, M_2, M_3 at the illustrated points in the figure (center point, or two end points of the upper middle member) as well as changes in temperature and moisture content on the whole structure. All sides have equal lengths $L_1 = L_2 = L_3 = L_4 = 0.25$ m, and four points are fixed as shown. Each member of the frame is a composite beam with any of the cross-sections illustrated in Fig. 3, and width $b = 0.02$ m. Four beam elements are used for each member, hence 96 beam elements (84 nodes) are used to model the 3D frame. The displacement of the load-application point of the laminated composite 3D frame in Fig. 15 (left) made of the two different composite laminates for applied P_3 and M_1 are presented in Fig. 16. Nastran tool will never yield answers for loads applied normal to the plane of the laminate. Hence, this problem cannot be solved using Nastran. Fig. 17 (left) shows the deformation of the laminated composite 3D frame structure with Laminate 3 cross section for the case of $P_3 = -10{,}000$ N.

The displacement and rotation of the center point of the upper middle member of the laminated composite 3D frame structure made laminates 3 and 4 for applied $P_{3.1} = P_{3.2}$ and $M_{1.1} = M_{1.2}$ loads at the two ends of the upper middle member are presented in Fig. 18. Fig. 17 (right) shows the deformation for the case of $P_{3.1} = P_{3.2} = 1{,}600{,}000$ N.

6. Conclusions

Combining Von Kármán's nonlinear theory with the composite lamination theory, and using a co-rotational element reference frame as the Updated Lagrangian formulation, an explicit expression of the tangent stiffness matrix of laminated composite beam element

undergoing large deformation and rotation has been obtained and utilized in analyzing different structures subjected to multiple mechanical and hygrothermal loads. The proposed approach has been verified by comparison with the results of Nastran and ANSYS finite element tools that enable modeling laminated composites, and the differences in the resulting displacements and rotations are less than 5% in all examples and cases. The developed beam element is much more efficient than using composite laminate tools in FEA software because of the ability to model such composites using 1D beam elements rather than 2D plate/shell or 3D solid elements. With structures undergoing large deformations, the computational time is less than 7% the time needed for solving the problem using Nastran shell elements and less than 21% using ANSYS 3D solid elements. The developed model will be very useful in modeling and designing flexible composites which have a lot of new applications, such as morphing aerospace structures and flexible robots.

Acknowledgment

The authors acknowledge the support of California State University, Northridge.

References

[1] Webber KG, Hopkinson DP, Lynch CS. Application of a classical lamination theory model to the design of piezoelectric composite unimorph actuators. J Intell Mater Syst Struct 2006;17(1):29–34.
[2] Khdeir AA, Aldraihem OJ. Exact analysis for static response of cross ply laminated smart shells. Compos Struct 2011;94(1):92–101.
[3] Khdeir AA, Aldraihem OJ. Analytical investigation of laminated arches with extension and shear piezoelectric actuators. Eur J Mech A Solids 2013;37:185–92.
[4] Han M-W, Rodrigue H, Kim H-I, Song S-H, Ahn S-H. Shape memory alloy/glass fiber woven composite for soft morphing winglets of unmanned aerial vehicles. Compos Struct 2016;140:202–12.
[5] Ahn S-H, Lee K-T, Kim H-J, Wu R, Kim J-S, Song S-H. Smart soft composite: an integrated 3D soft morphing structure using bend-twist coupling of anisotropic materials. Int J Precis Eng Manuf 2012;13(4):631–4.
[6] Wu R, Han M-W, Lee G-Y, Ahn S-H. Woven type smart soft composite beam with in-plane shape retention. Smart Mater Struct 2013;22(12):125007.
[7] Rodrigue H, Wang W, Bhandari B, Han M-W, Ahn S-H. Cross-shaped twisting structure using SMA-based smart soft composite. Int J Precis Eng Manuf-GT 2014;1(2):153–6.
[8] Kim H-J, Song S-H, Ahn S-H. A turtle-like swimming robot using a smart soft composite (SSC) structure. Smart Mater Struct 2013;22(1):014007.
[9] Han M-W, Rodrigue H, Cho S, Song S-H, Wang W, Chu W-S. Woven type smart soft composite for soft morphing car spoiler. 2016;86:285–98.
[10] Gordaninejad FF, Azhdari AA, Chalhoub NG. Nonlinear dynamic modelling of a revolute-prismatic flexible composite-material robot arm. ASME J Vib Acoust 1991;113(4):461–8.
[11] Grossard M, Chaillet N, Regnier S, editors. Flexible robotics: applications to multiscale manipulations. Wiley-ISTE; 2013. ISBN: 978-1-84821-520-7.
[12] Mororó LAT, de Melo AMC, Junior EP. Geometrically nonlinear analysis of thin-walled laminated composite beams. Latin Am J Solids Struct 2015;12:2094–117.
[13] Bhaskar K, Librescu L. A geometrically non-linear theory for laminated anisotropic thin-walled beams. Int J Eng Sci 1995;33(9):1331–44.
[14] Librescu L, Song O. Thin-walled composite beams: theory and application (solid mechanics and its applications). 1st ed. Springer; 2006.
[15] Omidvar B, Ghorbanpoor A. Nonlinear FE solution for thin-walled open-section composite beams. J Struct Eng 1996;122(11):1369–78.
[16] Cardoso JB, Benedito NM, Valido AJ. Finite element analysis of thin-walled composite laminated beams with geometrically nonlinear behavior including warping deformation. Thin-Walled Struct 2009;47(11):1363–72.
[17] Vo TP, Lee J. Geometrically nonlinear analysis of thin-walled open-section composite beams. Comput Struct 2010;88:347–56.
[18] Vo TP, Lee J. Geometrical nonlinear analysis of thin-walled composite beams using finite element method based on first order shear deformation theory. Arch Appl Mech 2011;81:419–35.
[19] Saravia CM. A large deformation–small strain formulation for the mechanics of geometrically exact thin-walled composite beams. Thin-Walled Structures 2014;84:443–51.
[20] Turkalj G, Lanc D, Brnic J, Pesic I. A beam formulation for large displacement analysis of composite frames with semi-rigid connections. Compos Struct 2015;134:237–46.
[21] Atluri SN. On some new general and complementary energy theorems for the rate problems in finite strain, classical elastoplasticity. J Struct Mech 1980;8(1):61–92.
[22] Atluri SN. Alternate stress and conjugate strain measures, and mixed variational formulations involving rigid rotations, for computational analyses of finitely deformed plates and shells: part-I: theory. Comput Struct 1984;18(1):93–116.
[23] Atluri SN, Cazzani A. Rotations in computational solid mechanics, invited feature article. Arch Comput Methods Eng, ICNME, Barcelona, Spain 1994;2(1):49–138.
[24] Atluri SN, Iura M, Vasudevan S. A consistent theory of finite stretches and finite rotations, in space-curved beams of arbitrary cross-section. Comput Mech 2001;27:271–81.
[25] Kondoh K, Tanaka K, Atluri SN. An explicit expression for the tangent-stiffness of a finitely deformed 3-D beam and its use in the analysis of space frames. Comput Struct 1986;24:253–71.
[26] Kondoh K, Atluri SN. Large-deformation, elasto-plastic analysis of frames under nonconservative loading, using explicitly derived tangent stiffnesses based on assumed stresses. Comput Mech 1987;2:1–25.
[27] Shi G, Atluri SN. Elasto-plastic large deformation analysis of spaceframes: a plastic-hinge and stress-based explicit derivation of tangent stiffnesses. Int J Numer Meth Eng 1988;26:589–615.
[28] Cai Y, Paik JK, Atluri SN. Large deformation analyses of space-frame structures, with members of arbitrary cross-section, using explicit tangent stiffness matrices, based on a Von Kármán type nonlinear theory in rotated reference frames. CMES 2009;53(2):117–45.
[29] Jones RM. Mechanics of composite materials. 2nd ed. Taylor and Francis; 1999.
[30] Bhati MA. Fundamental finite element analysis and applications: with mathematica and matlab computations. Wiley; 2005.